Intense tera-hertz laser driven proton acceleration in plasmas

A. Sharma,[1,a)] Z. Tibai,[2] and J. Hebling[2,3,4]
[1]ELI-ALPS, Szeged 6720, Hungary
[2]Institute of Physics, University of Pecs, Pecs 7624, Hungary
[3]Szentagothai Research Centre, University of Pecs, Pecs 7624, Hungary
[4]MTA-PTE High Field Terahertz Research Group, Pecs 7624, Hungary

(Received 4 May 2016; accepted 31 May 2016; published online 15 June 2016)

We investigate the acceleration of a proton beam driven by intense tera-hertz (THz) laser field from a near critical density hydrogen plasma. Two-dimension-in-space and three-dimension-in-velocity particle-in-cell simulation results show that a relatively long wavelength and an intense THz laser can be employed for proton acceleration to high energies from near critical density plasmas. We adopt here the electromagnetic field in a long wavelength (0.33 THz) regime in contrast to the optical and/or near infrared wavelength regime, which offers distinct advantages due to their long wavelength ($\lambda = 350\,\mu$m), such as the λ^2 scaling of the electron ponderomotive energy. Simulation study delineates the evolution of THz laser field in a near critical plasma reflecting the enhancement in the electric field of laser, which can be of high relevance for staged or post ion acceleration. *Published by AIP Publishing.* [http://dx.doi.org/10.1063/1.4953803]

When an intense laser light interacts with the plasma, the electrons acquire an exponential energy distribution with a mean energy of $k_B T_e = m_e c^2(\sqrt{(1+a_0^2)} - 1)$ due to the ponderomotive acceleration of electrons.[1] With intensities available today ($I = 10^{18} - 10^{21}\,\mathrm{W/cm^2}$, $\lambda = 1\,\mu$m), the ions hardly move in the electric field of the laser. As soon as the laser starts to tear off the electrons, its $e(\mathbf{v} \times \mathbf{B})$ force pushes electrons forward and electric field evolves due to the charge separation. The evolved longitudinal electric fields can be as high as the electric field of the laser itself but are stationary for the laser pulse duration, which is why they are called quasi-static. The relativistically intense lasers can accelerate ion beams from plasma to high energies (>MeV) in an extremely short distance. A recent development has demonstrated the laser driven acceleration of protons via different types of mechanisms, e.g., target-normal sheath acceleration (TNSA),[2–9] radiation pressure acceleration (RPA),[10–14] shock wave acceleration (SWA),[15–17] and relativistic transparency regime,[18–21] which are the center of experiments and theoretical investigations.

Acceleration of protons to high energy by a laser-plasma interaction is possible due to the production of hot electrons and the generation of very strong ambipolar fields. Hot electrons sheath production depends on large value of $I \times \lambda^2$ and on steep plasma density gradients, furthermore, the ion energy scales approximately with the irradiance $(I \times \lambda^2)^{1/2}$ (Ref. 7) of a laser. The ion energy dependence on irradiance of the laser field is the point of motivation in this article to focus towards the acceleration of protons driven by long wavelength (50–100 times longer than 800 nm−10 μm wavelength) Terahertz (THz) laser fields. Recent experimental investigation[16] on monoenergetic high-energy proton beam generation has attracted great deal of attention towards the long wavelength regime of particle acceleration. The experiment has demonstrated the generation of 20 MeV proton beam via the mechanism of collisionless shock acceleration driven by the 10 μm CO_2 laser interacting with a relatively low density gas-jet target.

Recent development for the generation of intense THz source has enabled many new applications such as THz-enhanced attosecond pulse generation,[22] undulation of relativistic electron bunches,[23,24] the post-acceleration of laser-driven protons and ions,[25] switching and controlling of magnetic domains.[26]

In the low-frequency THz spectral range (0.1–2 THz), the highest energy 0.4 mJ (Ref. 27) and the electric field of 1.2 MV/cm (Ref. 28) are obtained by optical rectification (OR) in lithium niobate (LN) with tilted-pulse-front pumping (TPFP). In the 2–10 THz range, 0.9 mJ with 42 MV/cm energy is produced in organic crystal by OR.[29]

In the high-frequency THz spectral range (10–100 THz), extremely high fields (100 MV/cm) are available.[30] In low-frequency THz range with TPFP technique, the THz energy will be increased beyond 1 mJ by using a high power pump pulse and cryogenic cooling of LN. By utilising the contact-grating technique[31] for TPFP, the THz pulse energy can be increased further. The recent development of high energy and high repetition rate laser sources (e.g., ELI-ALPS[32]) may provide the access to relativistic intense THz field.

In this investigation, we demonstrate the acceleration of protons via the interaction of low frequency (long wavelength), strong THz field with low density H_2 gas plasma. The irradiance of the THz field at 350 μm is estimated in the relativistic domain. We use the H_2 gas target for proton acceleration driven by intense THz laser field. The gas targets are better alternative to solid foils because of their operation at high repetition rate. For a 350 μm THz laser, the critical density is $10^{15}\mathrm{cm^{-3}}$, the plasma density in this range can be easily obtained by ionization of H_2 gas targets. The two-dimension-in-space and three-dimension-in-velocity (2D3V) particle-in-cell (PIC) simulations are performed with PIConGPU simulation CODE,[33,34] which is a fully

a)Email: ashutosh.sharma@eli-alps.hu

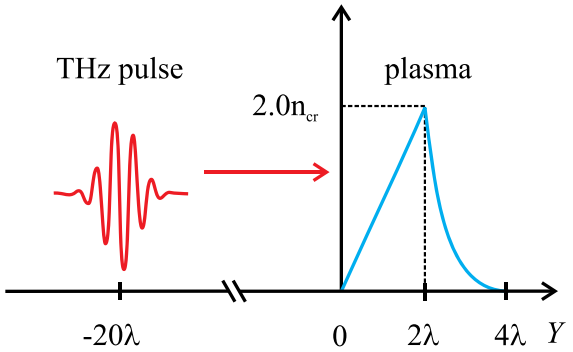

FIG. 1. The initial laser-plasma setup.

relativistic electromagnetic simulation code. It includes the utilities for data analysis and scripts for data visualization.[35–39] The PIC algorithm is used in PIConGPU to describe the kinetic plasma model. A charge-conserving current deposition algorithm is applied in electromagnetic limit to enable the integration of Maxwell's equations without any additional divergence correction. The instantaneous charge distribution is used to calculate the Poisson's equation at every time step in the electrostatic limit.

We start with a simulation while focusing the interaction of intense THz laser field with a preformed near critical density plasma. As shown in Fig. 1(a), we investigate the THz laser interaction with an inhomogeneous density plasma consisting of the linear density ramp followed by the exponentially decaying density profile. The density profile of preformed plasma considered here is similar to the experimentally measured plasma density profile of hydrogen gas jet.[16] In this study, linear density ramp and exponentially falling density profile are assumed of similar scale length to reduce the dissipation of shock field (which is responsible for high quality ion beam) through its propagation in exponential density profile. The THz field with a Gaussian intensity profile (in transverse direction along the x-axis) is incident on plasma target from left side and propagates in the y-direction. We consider a 4.6 ps linearly polarized laser pulse incident from the left side on the hydrogen plasma target. The dimensionless peak amplitude of the incident laser pulse is $a_0 = eE_0/m_e\omega c = 1$, where E_0 is the laser field amplitude, ω is the laser frequency, $\lambda = 350\,\mu$m is the laser wavelength, c is the light speed in a vacuum, and m_e and e are the electron mass and charge at rest, respectively. The focused radius of the laser is 5λ. The plasma length is 4λ. The plasma is assumed to be fully ionized into protons and electrons before the arrival of the main pulse. The peak plasma density is $n_e = 2.0n_{cr}$, where n_{cr} is the critical density corresponding to the laser frequency. The size of the simulation box is $(20 \times 51)\lambda^2$, and the cell number is 2048×5120. Each cell is filled with 2 protons and 2 electrons. Fig. 2 shows the electron (a)–(c)/ion (d)–(f) density at time instant $t = 29$ ps (a) and (d), $t = 233$ ps (b) and (e), and $t = 291$ ps (c) and (f), from two-dimensional (2D) particle-in-cell (PIC) simulations of the interaction of two-cycle

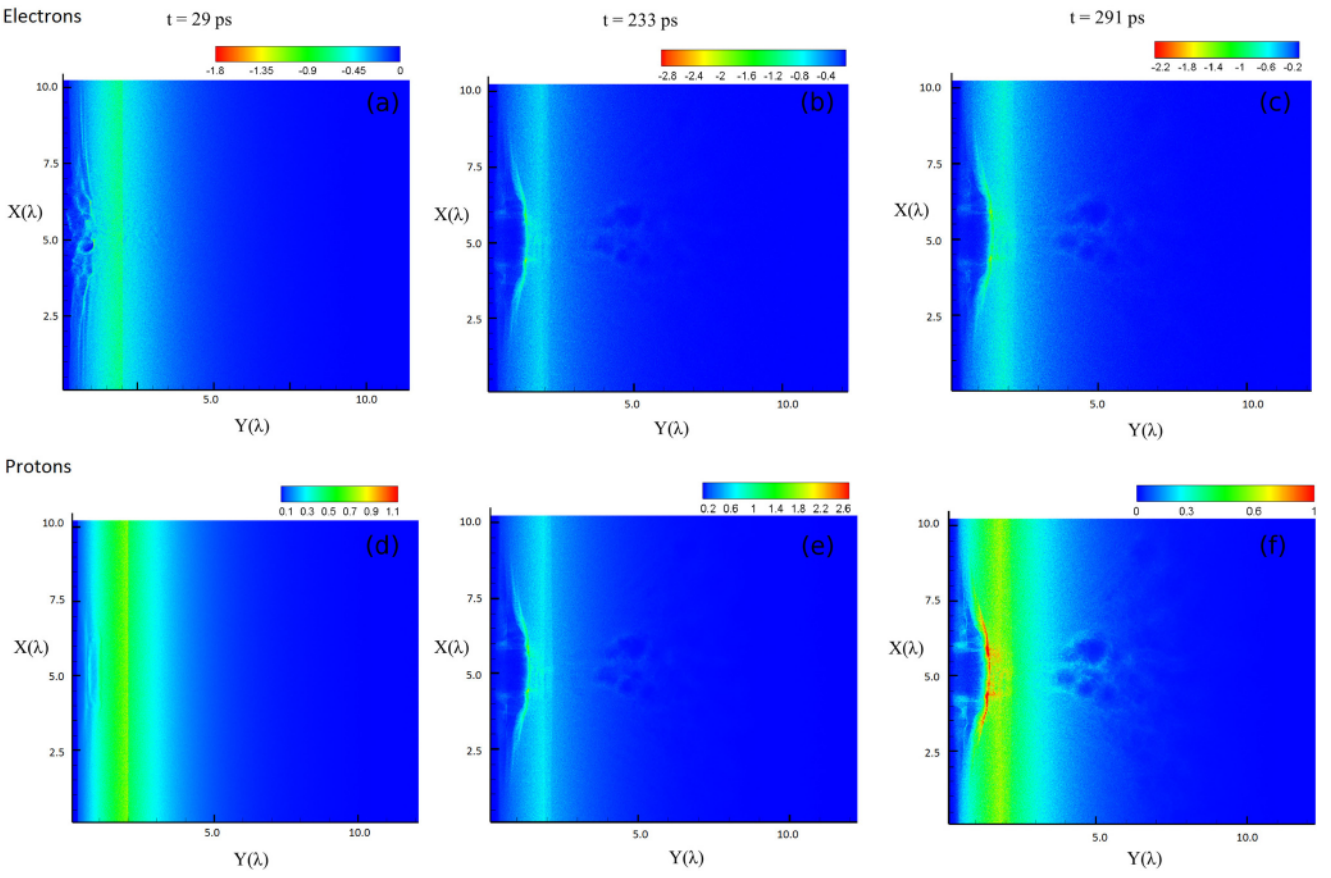

FIG. 2. The contour plot of the electron and ion density at time instant (a) and (d) 29 ps, (b) and (e) 233 ps, and (c) and (f) 291 ps; the colorbar shows the variation in electron/ion density where density is normalised with the critical density. The X and Y-axes are normalised with the laser wavelength $\lambda = 350\,\mu$m.

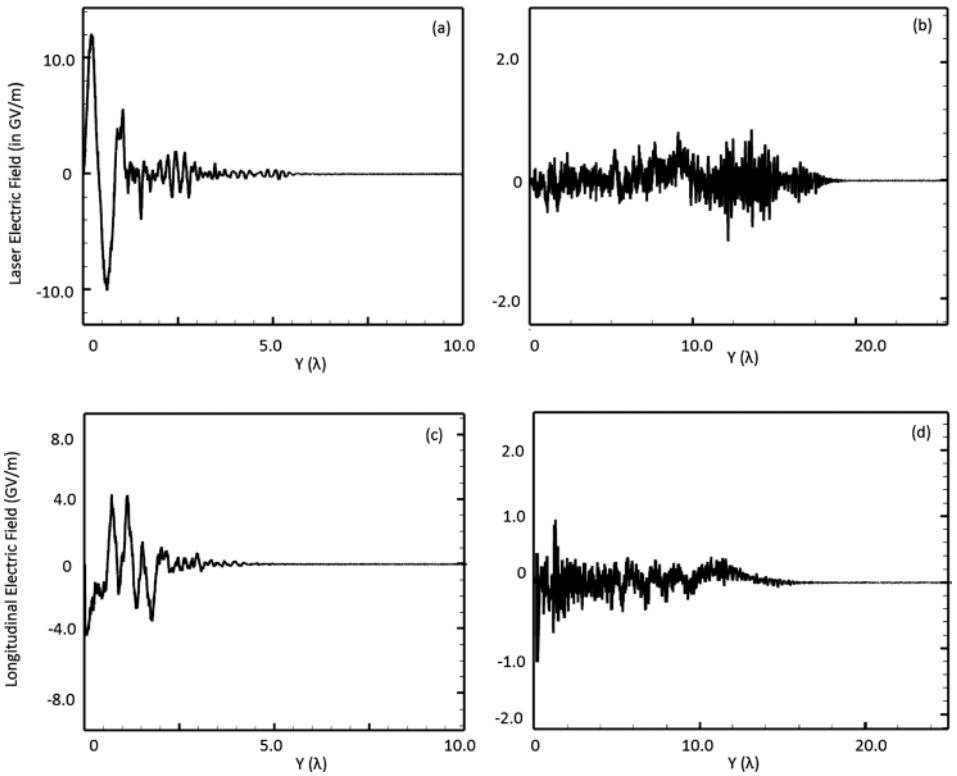

FIG. 3. Temporal evolution of electric field of laser and longitudinal electric field at $t = 233$ ps (a) and (c) and $t = 291$ ps (b) and (d).

duration, linearly polarized laser pulse with a hydrogen gas target having the inhomogeneous density profile with peak density $n_e = 2.0n_{cr}$. The plot shows that as the laser field propagates in the plasma from the underdense plasma region to the overdense region, it bores a hole in it. The hole depth increases with a velocity of $0.017\,c$. The hole boring velocity is estimated by balancing the momentum flux of the mass flow with the light pressure.[10]

Fig. 3 illustrates the evolution of electric field where the temporal evolution of laser electric field (a) and (b) and longitudinal electric field (c) and (d) is shown as the laser propagates along the propagation axis (Y-axis). The longitudinal electric field as shown in Figs. 3(c) and 3(d) corresponds to the evolution of shock field. Initially, plasma target with a linear density ramp is relativistically under-dense for the intense laser field ($a_0 = 1$); laser interacts with the significant volume of the target which allows the efficient heating of electrons. Hot electrons produced at the front surface propagate to the back of the target where the laser field is almost absent; return current electrons migrate to the left of the target, where they are heated by the laser field. The initial build-up of the return current together with the quick recirculation of the heated electrons due to the space charge field (Fig. 3(a)) at the front and the rear side of the target will lead to a uniform temperature profile, resulting in the generation of shock field (Fig. 3(b)) and ions reflection from it to high energy. As the transmitted laser field and shock field propagate further in the plasma and combine with the TNSA field at the rear side of the target, this superposition amplifies the accelerating field (Figs. 3(c) and 3(d)) at the rear side of the target, resulting in the higher proton energy.

In order to understand the energy distribution of accelerated protons at the rear side of the target, we show in Fig. 4 the distribution of proton energy density at 291 ps (a) and correspondingly the proton energy spectrum (b). We can see from the energy density distribution of protons that high energy protons are confined around the laser axis. The spectrum in Fig. 4 shows a peak at an energy of about 0.5 MeV,

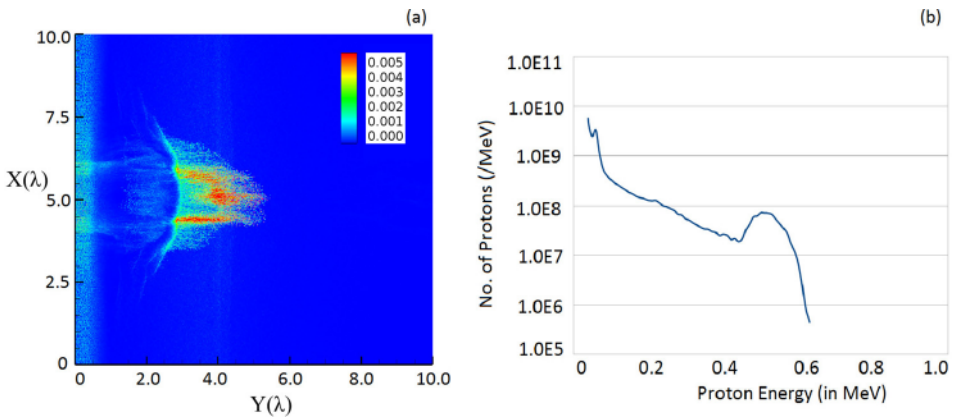

FIG. 4. Distribution of proton energy density (a) and proton energy spectrum (b), at time instant 291 ps.

corresponding to protons travelling near the axis; protons of lower energy are accelerated at the edges of the laser spot where the intensity is lower. We estimated from the simulation results the fraction of THz laser field absorption into the plasma as 0.6 (60%) which is close to the measured absorption[16,17] of short wavelength laser interacting with the gas target.

We further demonstrate the THz laser driven particle dynamics in underdense plasma followed by the overdense plasma region. The 2D PIC simulations are performed, considering the combined effect of underdense and overdense plasma density. The plasma density is linearly ramped from 0 to $1n_{cr}$, over a distance of 5λ, followed by a plasma of length one wavelength at density $1n_{cr}$ when the linear ramp approaches to the peak plasma density. The initial laser-plasma parameters are similar to the considered in previous simulation study. As the laser light approaches towards the peak density region, the field reflects from the critical surface and sets up a standing wave pattern. The plasma response to the resulting spatial variation of the ponderomotive force is to form periodic density depression. The density depressions collapse further while the density at the side of cavities increases more than the critical density. Such corrugated plasma surfaces, which are identical to the "bubble" structure formation as shown by Valeo and Estabrook[40] and by Lindman and Kindel *et al.*[41]

Fig. 5(a) shows the spatial distribution of ion density where the circular cavities can be seen with the radiation trapped inside it. These structures are accelerated due to the pressure associated with the intense field of focused THz laser in underdense plasma, while the perturbation near to the peak density surface is due to the electron dynamics in plasma in the region of underdense plasma just before the ions have a chance to move. Fig. 5(c) explains the longitudinal electric field associated with these structures along the propagation direction, which indicates the possibility of proton acceleration.

We also observed via the numerical simulation, spatio-temporal evolution of the THz laser pulse in a near critical density plasma and indicated the steepening of laser pulse which may provide the sharp rising, intense laser field for staged ion acceleration[42] and RPA ion acceleration.[43] We show in Figs. 6(a)–6(c) the spatio-temporal evolution of laser field in a homogeneous near critical density plasma $n_e = 0.1n_{cr}$ at different time instant along the laser propagation direction. Figs. 6(d)–6(f) show the evolution of the electric

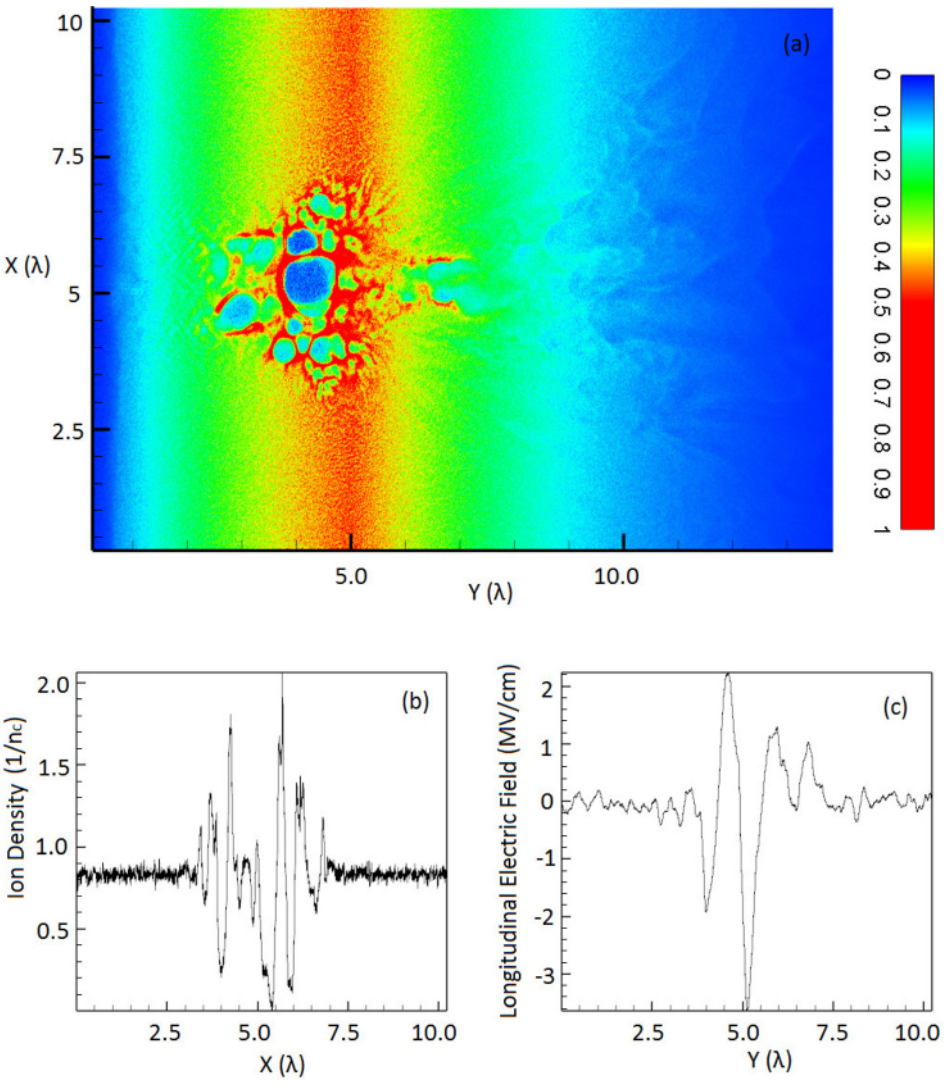

FIG. 5. (a)The spatial distribution of ion density at time instant 291 ps; the color bar shows the variation in density which is normalised with the critical density. (b) The variation of ion density normal to the direction of propagation (Y-axis) at time instant 291 ps around $Y = 5\lambda$. (c) The variation of longitudinal electric field along the propagation direction at time instant 291 ps around $X = 5\lambda$. The X and Y-axes are normalised with the laser wavelength $\lambda = 350\,\mu$m.

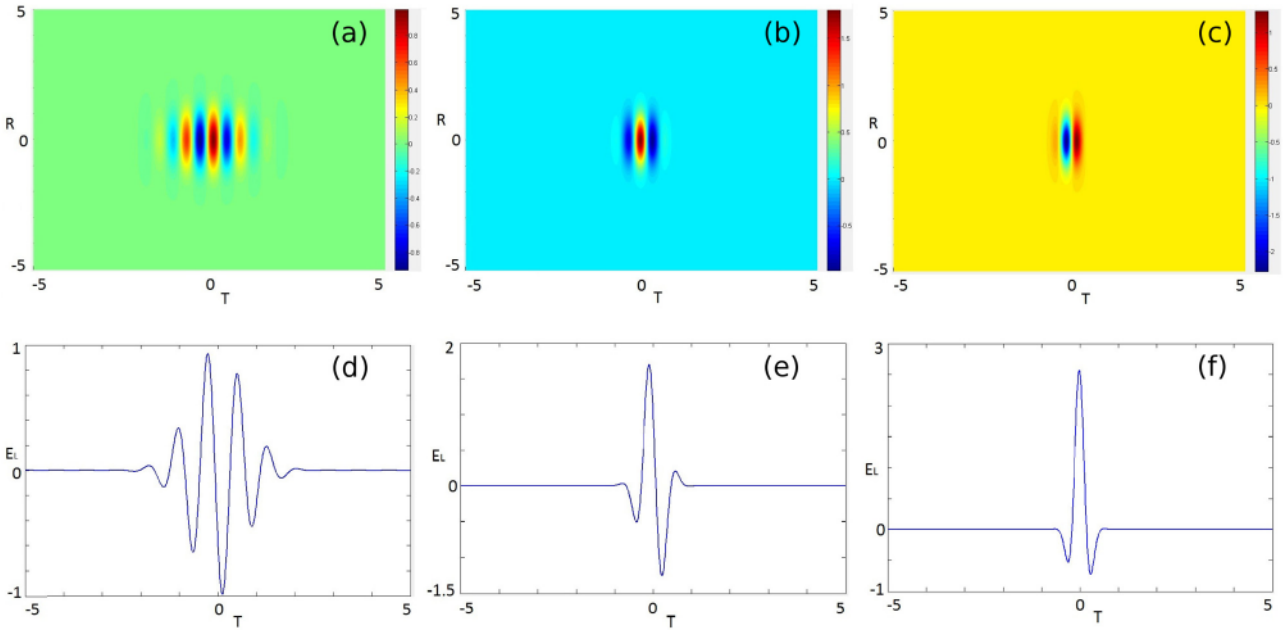

FIG. 6. The spatio-temporal evolution of the laser electric field along the propagation direction at different time instant (a)0 ps, (b) 29 ps, and (c) 60 ps. The temporal evolution of the electric field of laser at time instant (d) 0 ps, (e) 29 ps, and (f) 60 ps to demonstrate the steepening of laser pulse in a near critical density plasma. The x and y axes, respectively, present the T in time coordinate (normalised with the pulse length) and R in space coordinate (normalised with the beam radius). The color bar shows the variation in the normalized intensity.

field of THz laser at different time instant corresponding to the propagation distance in plasma, as shown in Figs. 6(a)–6(c). It is evident from the plots that there is shortening of pulse in temporal domain, because the high intensity part of the laser pulse travels faster than the front. The relativistic focusing and pulse shortening can be explained via the spatio-temporal evolution of refractive index of plasma under the relativistic intense field. Due to the relativistic effect, the refractive index of plasma modifies as $n_p = [1 - \gamma^{-1}(\omega_P/\omega)^2]^{1/2}$. Thus, there is a strong possibility to exploit the relativistic THz field to sharp rising, high contrast and high intensity laser field from the near critical density plasma, an ideal source field for post acceleration and in the regime of RPA.

In this study, we demonstrated the merits of a long-wavelength picosecond THz laser pulse for accelerating protons from a near critical density hydrogen plasma. We employ the particle-in-cell simulation to investigate the interaction of intense THz laser field with the near critical density plasma. In particular, we explored that wavelength scaling of the electron ponderomotive energy and critical plasma density may permit the production of high-quality proton beams via the interaction of a THz laser beam with a hydrogen gas target. The intensity of the THz laser was several orders of magnitude lower than the minimum required for producing protons of the same energy with a solid-state laser. The potential advantages of long-wavelength lasers as ion-beam drivers are based on the interplay of physical parameters, such as the ponderomotive energy conveyed to a charged particle by the laser field $(\sim\lambda^2)$, and the critical plasma-density $(\sim\lambda^{-2})$. In addition, the gas jet affords good control over the repetition rate and purity of the produced beams. The formation of bubble structures have also been shown to occur for plasma which has an initial density everywhere slightly less than the critical. Therefore, combining an intense THz laser field with a near critical density plasma target may offer a unique opportunity for a breakthrough. The THz laser driven proton acceleration can be enhanced further by employing the THz pulse train where initial interaction of a laser pulse with target will be utilised to heat the plasma electrons and driving the shock field. The post interaction of pulse train may enhance further the absorption and heating of plasma electrons which is responsible to drive the stable shock field to reflect the ions from it to high energies.

We performed PIC simulation utilising the code PIConGPU[33] in this research work. We acknowledge support of the Department of Information Services and Computing, Helmholtz-Zentrum Dresden-Rossendorf (HZDR), Germany; for providing access to the GPU Compute Cluster Hypnos. The authors also thank M. Bussmann, A. Huebl and the PIConGPU developer team for fruitful discussions regarding the simulation work; PIConGPU is developed and maintained by the Computational Radiation Physics Group at the Institute of Radiation Physics, HZDR.

[1]S. C. Wilks and W. L. Kruer, IEEE J. Quantum Electron. **33**, 1954 (1997).
[2]E. L. Clark, K. Krushelnick, J. R. Davies, M. Zepf, M. Tatarakis, F. N. Beg, A. Machacek, P. A. Norreys, M. I. K. Santala, I. Watts, and A. E. Dangor, Phys. Rev. Lett. **84**, 670 (2000).
[3]A. Maksimchuk, S. Gu, K. Flippo, D. Umstadter, and V. Yu. Bychenkov, Phys. Rev. Lett. **84**, 4108 (2000).
[4]R. A. Snavely, M. H. Key, S. P. Hatchett, T. E. Cowan, M. Roth, T. W. Phillips, M. A. Stoyer, E. A. Henry, T. C. Sangster, M. S. Singh, S. C. Wilks, A. MacKinnon, A. Offenberger, D. M. Pennington, K. Yasuike, A. B. Langdon, B. F. Lasinski, J. Johnson, M. D. Perry, and E. M. Campbell, Phys. Rev. Lett. **85**, 2945 (2000).
[5]S. C. Wilks, A. B. Langdon, T. E. Cowan, M. Roth, M. Singh, S. Hatchett, M. H. Key, D. Pennington, A. MacKinnon, and R. A. Snavely, Phys. Plasmas **8**, 542 (2001).

[6]P. Mora, Phys. Rev. Lett. **90**, 185002 (2003).
[7]J. Fuchs, P. Antici, E. d'Humieres, E. Lefebvre, M. Borghesi, E. Brambrink, C. A. Cecchetti, M. Kaluza, V. Malka, M. Manclossi, S. Meyroneinc, P. Mora, J. Schreiber, T. Toncian, H. Pepin, and P. Audebert, Nat. Phys. **2**, 48 (2006).
[8]L. Robson, P. T. Simpson, R. J. Clarke, K. W. D. Ledingham, F. Lindau, O. Lundh, T. McCanny, P. Mora, D. Neely, C.-G. Wahlström, M. Zepf, and P. McKenna, Nat. Phys. **3**, 58 (2007).
[9]T. E. Cowan, J. Fuchs, H. Ruhl, A. Kemp, P. Audebert, M. Roth, R. Stephens, I. Barton, A. Blazevic, E. Brambrink, J. Cobble, J. Fernández, J.-C. Gauthier, M. Geissel, M. Hegelich, J. Kaae, S. Karsch, G. P. Le Sage, S. Letzring, M. Manclossi, S. Meyroneinc, A. Newkirk, H. Pépin, and N. Renard-LeGalloudec, Phys. Rev. Lett. **92**, 204801 (2004).
[10]S. C. Wilks, W. L. Kruer, M. Tabak, and A. B. Langdon, Phys. Rev. Lett. **69**, 1383 (1992).
[11]A. P. L. Robinson, P. Gibbon, M. Zepf, S. Kar, R. G. Evans, and C. Bellei, Plasma Phys.: Controlled Fusion **51**, 024004 (2009).
[12]C. A. J. Palmer, N. P. Dover, I. Pogorelsky, M. Babzien, G. I. Dudnikova, M. Ispiriyan, M. N. Polyanskiy, J. Schreiber, P. Shkolnikov, V. Yakimenko, and Z. Najmudin, Phys. Rev. Lett. **106**, 014801 (2011).
[13]T. Esirkepov, M. Borghesi, S. V. Bulanov, G. Mourou, and T. Tajima, Phys. Rev. Lett. **92**, 175003 (2004).
[14]A. Macchi, F. Cattani, T. V. Liseykina, and F. Cornolti, Phys. Rev. Lett. **94**, 165003 (2005).
[15]L. O. Silva, M. Marti, J. R. Davies, R. A. Fonseca, C. Ren, F. S. Tsung, and W. B. Mori, Phys. Rev. Lett. **92**, 015002 (2004).
[16]D. Haberberger, S. Tochitsky, F. Fiuza, C. Gong, R. A. Fonseca, L. O. Silva, W. B. Mori, and C. Joshi, Nat. Phys. **8**, 95 (2012).
[17]F. Fiuza, A. Stockem, E. Boella, R. A. Fonseca, L. O. Silva, D. Haberberger, S. Tochitsky, W. B. Mori, and C. Joshi, Phys. Plasmas **20**, 056304 (2013).
[18]A. Henig, D. Kiefer, K. Markey, D. C. Gautier, K. A. Flippo, S. Letzring, R. P. Johnson, T. Shimada, L. Yin, B. J. Albright, K. J. Bowers, J. C. Fernández, S. G. Rykovanov, H.-C. Wu, M. Zepf, D. Jung, V. Kh. Liechtenstein, J. Schreiber, D. Habs, and B. M. Hegelich, Phys. Rev. Lett. **103**, 045002 (2009).
[19]D. Jung, L. Yin, B. J. Albright, D. C. Gautier, S. Letzring, B. Dromey, M. Yeung, R. Hörlein, R. Shah, S. Palaniyappan, K. Allinger, J. Schreiber, K. J. Bowers, H. C. Wu, J. C. Fernandez, D. Habs, and B. M. Hegelich, New J. Phys. **15**, 023007 (2013).
[20]L. Yin, B. J. Albright, K. J. Bowers, D. Jung, J. C. Fernandez, and B. M. Hegelich, Phys. Rev. Lett. **107**, 045003 (2011).
[21]M. Roth, D. Jung, K. Falk, N. Guler, O. Deppert, M. Devlin, A. Favalli, J. Fernandez, D. Gautier, M. Geissel, R. Haight, C. E. Hamilton, B. M. Hegelich, R. P. Johnson, F. Merrill, G. Schaumann, K. Schoenberg, M. Schollmeier, T. Shimada, T. Taddeucci, J. L. Tybo, F. Wagner, S. A. Wender, C. H. Wilde, and G. A. Wurden, Phys. Rev. Lett. **110**, 044802 (2013).
[22]K. Kovacs, E. Balogh, J. Hebling, V. Tosa, and K. Varju, Phys. Rev. Lett. **108**, 193903 (2012).
[23]J. Hebling, J. A. Fulop, M. I. Mechler, L. Palfalvi, C. Toke, and G. Almasi, e-print arXiv:11096852 (2011).
[24]L. J. Wong, A. Fallahi, and F. X. Kartner, Opt. Express **21**, 9792 (2013).
[25]L. Palfalvi, J. A. Fulop, G. Toth, and J. Hebling, Phys. Rev. ST Accel. Beams **17**, 031301 (2014).
[26]C. Vicario, C. Ruchert, F. Ardana-Lamas, P. M. Derlet, B. Tudu, J. Luning, and C. P. Hauri, Nat. Photonics **7**, 720 (2013).
[27]J. A. Fulop, Z. Ollmann, C. Lombosi, C. Skrobol, S. Klingebiel, L. Palfalvi, F. Krausz, S. Karsch, and J. Hebling, Opt. Express **22**, 20155 (2014).
[28]H. Hirori, A. Doi, F. Blanchard, and K. Tanaka, Appl. Phys. Lett. **98**, 091106 (2011).
[29]C. Vicario, A. V. Ovchinnikov, S. I. Ashitkov, M. B. Agranat, V. E. Fortov, and C. P. Hauri, Opt. Lett. **39**, 6632 (2014).
[30]A. Sell, A. Leitenstorfer, and R. Huber, Opt. Lett. **33**, 2767 (2008).
[31]Z. Ollmann, J. Hebling, and G. Almasi, Appl. Phys. B **108**, 821 (2012).
[32]See http://www.eli-alps.hu for ELI-ALPS.
[33]M. Bussmann, H. Burau, T. E. Cowan, A. Debus, A. Huebl, G. Juckeland, T. Kluge, W. E. Nagel, R. Pausch, F. Schmitt, U. Schramm, J. Schuchart, and R. Widera, Proc. Int. Conf. High Performance Comp., Networking, Storage Anal. **5-1** (2013).
[34]H. Burau, R. Widera, W. Honig, G. Juckeland, A. Debus, T. Kluge, U. Schramm, T. E. Cowan, R. Sauerbrey, and M. Bussmann, IEEE Trans. Plasma Sci. **38**, 2831 (2010).
[35]M. A. Heald and C. B. Wharton, *Plasma Diagnostics with Microwaves* (John Wiley Press, New York, 1965).
[36]S. Okajima, K. Nakayama, and H. Tazawa, Rev. Sci. Instrum. **72**, 1094 (2001).
[37]J. Ropcke, L. Mechold, and M. Kaning, Rev. Sci. Instrum. **71**, 3706 (2000).
[38]M. R. Siegrist, H. Bindslev, and R. Brazis, Infrared Phys. Technol. **40**, 247 (1999).
[39]R. Bista, H. Merabet, R. Bruch, and S. Fulling, Nucl. Instrum. Methods B **261**, 166 (2007).
[40]E. J. Valeo and K. G. Estabrook, Phys. Rev. Lett. **34**, 1008 (1975); K. Estabrook, Phys. Fluids **19**, 1733 (1976).
[41]E. L. Lindman, J. Phys. (Paris), Colloq., Suppl. **12**, 38, C6-9 (1977); J. M. Kindel *et al*., in Proceedings of the U.S.-Japan Seminar on Theory and Applications of Multi-Ionized Plasmas Produced by Laser and Particle Beams, Nara, Japan, 3–7 May 1982.
[42]Y. J. Gu, Z. Zhu, X. F. Li, Q. Yu, S. Huang, F. Zhang, Q. Kong, and S. Kawata, Phys. Plasmas **21**, 063104 (2014).
[43]J. H. Bin, W. J. Ma, H. Y. Wang, M. J. V. Streeter, C. Kreuzer, D. Kiefer, M. Yeung, S. Cousens, P. S. Foster, B. Dromey, X. Q. Yan, R. Ramis, J. Meyer-ter-Vehn, M. Zepf, and J. Schreiber, Phys. Rev. Lett. **115**, 064801 (2015).